arXiv:0912.5491v1 [astro-ph.SR] 30 Dec 2009

Angular Diameters and Effective Temperatures of Twenty-five K Giant Stars from the CHARA Array

Ellyn K. Baines[†]

Remote Sensing Division, Naval Research Laboratory, 4555 Overlook Avenue SW, Washington, DC 20375

ellyn.baines.ctr@nrl.navy.mil

Michaela P. Döllinger

ESO, Karl-Schwarzschild-Strasse 2, D-85748 Garching bei München, Germany

Felice Cusano, Eike W. Guenther, Artie P. Hatzes

Thüringer Landessternwarte Tautenburg, Sternwarte 5, D-07778 Tautenburg, Germany

Harold A. McAlister, Theo A. ten Brummelaar, Nils H. Turner, Judit Sturmann, Laszlo Sturmann, P. J. Goldfinger, Christopher D. Farrington

Center for High Angular Resolution Astronomy, Georgia State University, P.O. Box 3969, Atlanta, GA 30302-3969

Stephen T. Ridgway

Kitt Peak National Observatory, National Optical Astronomy Observatory, P.O. Box 26732, Tucson, AZ 85726-6732

ABSTRACT

Using Georgia State University's CHARA Array interferometer, we measured angular diameters for 25 giant stars, six of which host exoplanets. The combination of these measurements and *Hipparcos* parallaxes produce physical linear radii for the sample. Except for two outliers, our values match angular diameters and physical radii estimated using photometric methods to within the associated errors with the advantage that our uncertainties are significantly lower. We also calculated the effective temperatures for the stars using the newly-measured diameters. Our values do not match those derived from spectroscopic observations as well, perhaps due to the inherent properties of the methods used or because of a missing source of extinction in the stellar models that would affect the spectroscopic temperatures.

[†]Some of the observations described here was completed while with the Center for High Angular Resolution Astronomy, Georgia State University, P.O. Box 3969, Atlanta, GA 30302-3969.

Subject headings: infrared: stars — planetary systems — stars: fundamental parameters — techniques: interferometric, spectroscopic

1. Introduction

Giant star radii have been measured in the past using various interferometers, including the Mark III (85 giants and supergiants, Mozurkewich et al. 2003), the Palomar Testbed Interferometer (69 giants and supergiants, van Belle et al. 1999), the Navy Prototype Optical Interferometer (50 giants and supergiants, Nordgren et al. 1999), and the Center for High Angular Resolution Astronomy (CHARA) Array (4 Hyades giants, Boyajian et al. 2009). These measurements are valuable because these are the stars populating the coolest, most luminous part of the Hertzsprung-Russell (H-R) diagram (van Belle et al. 1999). What makes the sample of giant stars under consideration here particularly interesting is that they are potential exoplanet hosts, and planetary candidates have been discovered around six of the stars already.

Two important characteristics of a star are its mass and radius. For giant stars, the determination of these parameters is indirect and heavily model dependent. In practice, spectroscopic observations to measure the surface gravities ($\log g$), effective temperatures ($T_{\rm eff}$), and iron abundances ([Fe/H]) can be combined with a distance measurement to derive the stellar radius. Fitting evolutionary tracks to the position of the star in the H-R diagram then yields the mass. The reliability of these measurements depend both on the validity of the model atmospheres and the stellar evolution code. Unfortunately this is an uncertain process because the evolutionary tracks of stars with a wide range of masses all converge to near the same region of the H-R diagram as they evolve up the giant branch. In particular the mass estimates derived from evolutionary tracks depend critically on several parameters hidden in the tracks, such as the mixing length parameter and its assumed constancy for all stars, the unknown helium content in the core, and uncertainties about the nature of the convection zone. As a result, using different tracks can produce different masses, and in the absence of good calibrating objects no set of tracks can be claimed to provide the best results. On the other hand, if one can test and calibrate these evolutionary tracks by comparing the theoretically-determined mass and radius to observed values, then one can have some faith in applying these tracks to stars for which direct measurements of these stellar parameters is not possible.

A star's mass is not only important for its evolution, but it should play an important role in the type of planetary system a star will form. There are a number of Doppler surveys searching for planets around evolved giant stars with stellar masses of 1 to 2 $M_{\odot}$ (e.g., Niedzielski et al. 2009; Döllinger et al. 2007; Setiawan et al. 2005; Sato et al. 2005). All are plagued by the same problem in that they rely on evolutionary tracks to determine the stellar mass. Until these are calibrated both the mass of the host star and the planet are uncertain.

A more reliable means of calculating the stellar mass independent of evolutionary tracks and

model atmospheres is using stellar oscillation observations, as the frequency of stellar oscillations is related to the mean density of the star. If one has an accurate stellar radius it is simple to compute a stellar mass from the oscillation frequencies that is model independent. Depending on the accuracy of the diameter measurements, the masses can be measured to an accuracy of ∼2% (Teixeira et al. 2009) to ∼15% (Hatzes & Zechmeister 2007).

There is increasing evidence that most and possibly all giant stars show stellar oscillations (e.g., de Ridder et al. 2006; Frandsen, et al. 2002; Hatzes & Cochran 1994), which are due to p-mode oscillations where pressure is the restoring force. Thus giant stars are an ideal class of objects for deriving fundamental stellar parameters. They are abundant, they have large angular diameters suitable for interferometric measurements, and they exhibit stellar oscillations with radial velocity amplitudes of a few to several tens of m/s, which are easily measurable by state-of-the-art techniques. The observed oscillation frequencies constrain the internal structure of the star (Bedding et al. 2006) and interferometry measures the star's size, and the combination leads to the mass of the star. Once stellar isochrones have been refined and calibrated for these evolved stars, they can be used to determine the masses of all planet-hosting giant stars. Because collecting data on the oscillation frequencies requires considerable telescope resources and can only be done for relatively few stars, we first present our results on interferometric measurements on a larger sample of giant stars.

The advantage interferometry provides is the ability to directly measure stellar angular diameters. Once the angular diameters are known for these giant stars, physical radii and effective temperatures can be calculated when combined with other parameters, such as the parallax, bolometric flux, interstellar absorption, and bolometric corrections. The radii and effective temperatures are important values that characterize the parent star as well as the environment in which the exoplanet resides for those stars hosting planets. Section 2 describes the spectroscopic measurements of $T_{\rm eff}$ and log g for the sample, §3 discusses the interferometric observations, §4 explains how the angular diameters, linear radii, and $T_{\rm eff}$ were determined, and §5 explores the physical implications of the interferometric observations.

2. Spectroscopic observations

Our sample of K giant stars were obtained from the planet search survey of Döllinger et al. (2007). As part of this program the $T_{\rm eff}$ and log g were measured, which allowed us to estimate the stellar radii and masses. Table 1 lists the 25 stars observed here, and planets have already been found orbiting HD 73108 (Döllinger et al. 2007), HD 139357 and HD 170693 (Döllinger et al. 2009a), HD 32518 and HD 136726 (Döllinger et al. 2009b), and HD 167042 (Johnson et al. 2008; Sato et al. 2008; Döllinger et al. 2009c). Three additional stars show long-period variations in their radial velocity measurements: HD 106574, HD 157681, and HD 200205 (Döllinger et al. 2009d). The targets chosen for our observing list are bright ($V < 6.5$) giant stars that showed significant short-term variability indicative of stellar pulsations, which made them excellent candidates for

both stellar oscillation observations and interferometric measurements.

The spectroscopic observations were carried out using the Coudé Échelle spectrograph of the 2-m-Alfred Jensch telescope of the Thüringer Landessternwarte Tautenburg. The spectrograph has a resolving power of $\Delta\lambda/\lambda = 67000$ and the wavelength range used was 4700 to 7400 Å. Standard IRAF routines were used for subtracting the bias offset, flat-fielding, subtracting the scattered light, extracting the spectra, and for the wavelength calibration[1].

In order to determine the stellar parameters from the spectra, a grid of model atmospheres from Gustafsson et al. (1975) was used in which a plane-parallel atmosphere in local thermodynamic equilibrium was assumed. We selected 144 unblended Fe I and 8 Fe II lines in the wavelength range 5806 and 6858 Å using the line list of Pasquini et al. (2004). The iron abundance [Fe/H] was determined by assuming that Fe I lines of different equivalent widths have to give the same relative abundance of iron. For the effective temperature, an excitation equilibrium of Fe I and Fe II for lines of different excitation potentials was used, and the surface gravity was determined from the ionization balance of Fe I to Fe II lines (Döllinger 2008). The resulting [Fe/H], $T_{\rm eff}$, and log g values are listed in Table 1.

3. Interferometric observations

Interferometric observations were obtained using the CHARA Array, a six element optical-infrared interferometer located on Mount Wilson, California (ten Brummelaar et al. 2005). All observations used the pupil-plane "CHARA Classic" beam combiner in the K'-band at 2.15 μm while visible wavelengths (470-800 nm) were used for tracking and tip/tilt corrections. The observing procedure and data reduction process employed here are described in McAlister et al. (2005).

We interleaved calibrator and target star observations so that every target was flanked by calibrator observations made as close in time as possible, which allowed us to convert instrumental target and calibrator visibilities to calibrated visibilities for the target. Reliable calibrators were chosen to be single stars with expected visibility amplitudes >85% so they were nearly unresolved on the baselines used, which meant uncertainties in the calibrator's diameter did not affect the target's diameter calculation as much as if the calibrator star had a significant angular size. In a few cases, a calibrator had a stellar companion but at such a distance that light from the secondary star would not contaminate our interferometric measurements and the calibrator could therefore be treated as a single star.

To check for possible unseen close companions that would contaminate our observations, we created spectral energy distribution (SED) fits based on published $UBVRIJHK$ photometric values obtained from the literature for each calibrator to establish diameter estimates. This also

[1]IRAF is distributed by the National Optical Astronomy Observatories, which are operated by the Association of Universities for Research in Astronomy, Inc., under cooperative agreement with the National Science Foundation.

allowed us to see if there was any excess emission associated with a low-mass stellar companion or circumstellar disk. Calibrator candidates showing displaying variable radial velocities or any other indication of companions were discarded.

We used Kurucz model atmospheres[2] based on $T_{\rm eff}$ and log g values to calculate limb-darkened angular diameters for the calibrators. The stellar models were fit to observed photometry after converting magnitudes to fluxes using Colina et al. (1996) for $UBVRI$ values and Cohen et al. (2003) for JHK values. See Table 2 for the $T_{\rm eff}$ and log g used and the resulting limb-darkened angular diameters.

4. Determination of angular diameter and $T_{\rm eff}$

The observed quantity of an interferometer is defined as the visibility (V), which is fit to a model of a uniformly-illuminated disk (UD) that represents the observed face of the star. Diameter fits to V were based upon the UD approximation given by $V = [2J_1(x)]/x$, where J_1 is the first-order Bessel function and $x = \pi B \theta_{\rm UD} \lambda^{-1}$, where B is the projected baseline at the star's position, $\theta_{\rm UD}$ is the apparent UD angular diameter of the star, and λ is the effective wavelength of the observation (Shao & Colavita 1992). A more realistic model of a star's disk involves limb-darkening (LD), and relationship incorporating the linear limb darkening coefficient μ_λ (Hanbury-Brown et al. 1974) is:

$$V = \left(\frac{1-\mu_\lambda}{2} + \frac{\mu_\lambda}{3}\right)^{-1} \times \left[(1-\mu_\lambda)\frac{J_1(\mathrm{x})}{\mathrm{x}} + \mu_\lambda \left(\frac{\pi}{2}\right)^{1/2} \frac{J_{3/2}(\mathrm{x})}{\mathrm{x}^{3/2}}\right]. \quad (1)$$

Table 3 lists the Modified Julian Date (MJD), projected baseline (B) at the time of observation, projected baseline position angle (Θ), calibrated visibility (V_c), and error in V_c (σV_c) for each giant star observed. Figures 1 through 3 show the LD diameter fits for all the stars.

The limb-darkening coefficient was obtained from Claret et al. (1995) after adopting the $T_{\rm eff}$ and log g values required for each star observed. The resulting LD angular diameters are listed in Table 4. The average difference between the UD and LD diameters are on the order of a few percent, and the final angular diameters are little affected by the choice of μ_λ. All but four stars have $\theta_{\rm LD}$ errors of 2% or less, three of the four have errors of only 3%, and the final star has a 5% error. Additionally, the combination of the interferometric measurement of the star's angular diameter plus the *Hipparcos* parallax (van Leeuwen 2007) allowed us to determine the star's physical radius. The results are also listed in Table 4. In principle, one can calculate the mass of each star from the physical radius and log g values. However, the formal errors in log g lead to errors in such mass estimates near the 50% level, thereby significantly decreasing their usefulness to this analysis.

For each $\theta_{\rm LD}$ fit, the errors were derived via the reduced χ^2 minimization method (Wall & Jenkins 2003; Press et al. 1992): the diameter fit with the lowest χ^2 was found and the corresponding diam-

[2]Available to download at http://kurucz.cfa.harvard.edu.

eter was the final $\theta_{\rm LD}$ for the star. The errors were calculated by finding the diameter at χ^2+1 on either side of the minimum χ^2 and determining the difference between the χ^2 diameter and χ^2+1 diameter. In calculating the diameter errors in Table 4, we adjusted the estimated visibility errors to force the reduced χ^2 to unity because when this is omitted, the reduced χ^2 is well under 1.0, indicating we are overestimating the errors in our calibrated visibilities.

Limb-darkened angular diameters were estimated using the relationship described in Kervella et al. (2004) between the $(V-K)$ color and log $\theta_{\rm LD}$ (see $\theta_{\rm estimate}$ in Table 1). The table also lists $R_{\rm estimate}$, which were derived using $\theta_{\rm estimate}$ and the stars' parallaxes. The major weakness of this method lies in the uncertainties surrounding the K-magnitudes, which were taken from two sources: *The Two-Micron Sky Survey* (TMSS, Neugebauer & Leighton 1969, errors ∼2-5%) and *The 2MASS All-Sky Catalog of Point Sources* (2MASS, Cutri et al. 2003, errors ∼6-12%). Preference was given to the former because 2MASS measurements saturate at magnitudes brighter than ∼3.5 in the K-band even when using the shortest exposure time[3]. The large errors associated with 2MASS magnitudes for these bright stars led to large errors in angular diameter and physical radii estimates.

Once $\theta_{\rm LD}$ was determined interferometrically, the $T_{\rm eff}$ was calculated using the relation

$$F_{\rm BOL} = \frac{1}{4}\theta_{\rm LD}^2 \sigma T_{\rm eff}^4, \tag{2}$$

where $F_{\rm BOL}$ is the bolometric flux and σ is the Stefan-Bolzmann constant. The stars' V and K magnitudes were dereddened using the extinction curve described in Cardelli et al. (1989) and interstellar absorption ($A_{\rm V}$) values were from Famaey et al. (2005) except for HD 113049 and HD 176408, which had no $A_{\rm V}$ in the literature. $A_{\rm V}$ values for these two stars were estimated through a non-linear, least squares fit and a reddening prescription from Fitzpatrick (1999), who presented a wavelength-dependent extinction curve. The intrinsic broad-band color $(V-K)$ was calculated and bolometric corrections (BCs) were determined by interpolating between the [Fe/H] = +0.2, 0.0, and -1.0 tables found in Alonso et al. (1999). They point out that in the range of 6000 K $\geq T_{\rm eff} \geq$ 4000 K, their BC calibration is symmetrically distributed around a ±0.10 magnitude band when compared to other calibrations. The average BC used here is 0.55, and because 0.10 is 18% of 0.55, we assigned a 18% error bar to our BC values. The bolometric flux was determined by applying the BC for each star and the $T_{\rm eff}$ was calculated (see Table 4). All $T_{\rm eff}$ errors are ≤ 4%, 11 stars have errors of ≤ 2%, and the major source of error in calculating $T_{\rm eff}$ stemmed, again, from uncertainties in K-magnitudes.

Giant star masses were estimated using the PARAM stellar model[4] from Girardi et al. (2000) with a modified version of the method described in da Silva et al. (2006). The input parameters for each star were its interferometrically-measured $T_{\rm eff}$, its spectroscopically-derived [Fe/H], its V

[3]Explanatory Supplement to the 2MASS All Sky Data Release and Extended Mission Products, http://www.ipac.caltech.edu/2mass/releases/allsky/doc/.

[4]http://stev.oapd.inaf.it/cgi-bin/param_1.0

magnitude from Mermilliod (1991), and its Hipparcos parallax (van Leeuwen 2007) along with the corresponding error for each value. The model used these inputs to estimate each star's age, mass, radius, $(B-V)_0$, and log g using the isochrones and a Bayesian estimating method, calculating the probability density function separately for each property in question. da Silva et al. qualify mass estimates as "more uncertain" than other properties, so the resulting masses listed in Table 1 should be viewed as a rough estimates only.

5. Results and discussion

In order to check how well the estimated and measured angular diameters agreed, we plotted photometrically-estimated versus interferometrically-measured angular diameters in Figure 4, and Figure 5 shows a similar plot for physical radii. The angular diameters determined using K-band photometry from 2MASS show generally higher errors in Figure 4 than the diameters determined using TMSS photometry. This plot clearly shows the advantage of measuring angular diameters interferometrically, as the errors are significantly smaller than the photometric estimates in all cases. There is an even scatter around the 1:1 ratio line, and all but two stars are within 1σ of the line.

The outliers in both Figures 4 and 5 are HD 118904 and HD 157681. Neither star shows any sign of binarity in the literature, and the SEDs created using the $T_{\rm eff}$ and log g based on their spectral type and Cox (2000) do not show any excess in the infrared wavelengths that would suggest a low-mass stellar companion or a circumstellar disk. In both cases, the problem may lie with the calibrator stars chosen. HD 157681 was observed using the calibrator HD 158460, and though the latter has a small estimated diameter (0.268±0.016 mas) and its SED shows no excess flux in the infrared that would indicate a low-mass stellar companion or circumstellar disk, HD 157681 was the only star observed with that calibrator and there could be an unseen companion that is not taken into account when estimating the star's diameter. Future observations of HD 157681 with different calibrators will make the situation clearer.

HD 118904 was observed using HD 124063 as a calibrator, and the same calibrator was used to observe the target star HD 113049 along with the second calibrator HD 107193. When the data were calibrated separately for HD 113049, the diameters showed a 0.08 mas difference, which is on the order of an 8% change. If HD 118904's diameter is reduced by 8%, the data point is within errors on the 1:1 ratio line for both plots in Figures 4 and 5. Because this is the case, only HD 107193 was used in the calibration of HD 113049's data, and the angular diameter, radius, and $T_{\rm eff}$ listed in Table 4 are based on those data alone.

Figure 5 shows that while a fair number of photometric and interferometric radii agree very well, there are some that show slight discrepancies, notwithstanding the error bars. This could be due to a few different effects. First, the photometrically-determined radii depend on temperature estimates that may not be correct. If the star is highly active or there is a very faint companion,

these could affect the temperature and therefore radii estimates[5]. Second, the limb-darkening law used to determine interferometric diameters and radii may not take certain stellar features into account, such as starspots or extremely active regions. This would not be a large effect because even altering the limb-darkening coefficient μ_λ by 20% changes the limb-darkened angular diameter by an average of 0.7%. Third, the differences may be due to changes in the stars' convections zones, because as the star evolves the convection zone gets deeper. Convection is not well modeled, which may lead to errors in the photometric radii estimates.

We also plotted the interferometrically-measured $T_{\rm eff}$ versus those derived spectroscopically in Figure 6. There is some scatter off the 1:1 ratio line, particularly for the cooler stars. The errors in $T_{\rm eff}$ do not show a trend with log g, diameter, radius, $(V-K)$ color, distance, spectral type, metallicity, or bolometric correction. The discrepancies may be due to the inherent properties of the methods used to measure $T_{\rm eff}$. Spectroscopic values are based on Fe I and Fe II lines and measure the $T_{\rm eff}$ in the part of the atmosphere where those lines are present, while interferometry calculates the overall $T_{\rm eff}$ of the star using the measured diameter. It has been surmised that atmospheric models of K giant stars in the near-ultraviolet band are missing a source of thermal extinction, which would also affect the $T_{\rm eff}$ measurements (Short & Hauschildt 2009).

Our next step will be to determine the oscillation frequencies of these stars so that we can compare the true masses of these stars with those estimated using evolutionary models.

Many thanks to Douglas Gies for his help and advice. The CHARA Array is funded by the National Science Foundation through NSF grant AST-0606958 and by Georgia State University through the College of Arts and Sciences, and STR acknowledges partial support by NASA grant NNH09AK731. We are also grateful to the user support group of the Alfred-Jensch telescope. This research has made use of the SIMBAD database, operated at CDS, Strasbourg, France. This publication makes use of data products from the Two Micron All Sky Survey, which is a joint project of the University of Massachusetts and the Infrared Processing and Analysis Center/California Institute of Technology, funded by the National Aeronautics and Space Administration and the National Science Foundation.

REFERENCES

Allende Prieto & Lambert 1999, A&A, 352, 555

Alonso, A., Arribas, S., & Martínez-Roger, C. 1999, A&AS, 140, 261

Bedding, T. R., et al. 2006, ApJ, 647, 558

[5]If a second star is present and is more than ∼2.5 magnitudes fainter than the host star, the effects of the secondart star will be not seen in interferometric observations and would therefore have no effect on the angular diameter or physical radii measurements.

Boyajian, T. S., et al. 2009, ApJ, 691, 1243

Cardelli, J. A., Clayton, G. C., & Mathis, J. S. 1989, ApJ, 345, 245

Claret, A., Diaz-Cordoves, J., & Gimenez, A. 1995, A&AS, 114, 247

Cohen, M., Wheaton, W. A., & Megeath, S. T. 2003, AJ, 126, 1090

Colina, L., Bohlin, R. C., & Castelli, F. 1996, AJ, 112, 307

Cox, A. N. 2000, Allen's astrophysical quantities, 4th ed., ed. A. N. Cox (New York: AIP Press; Springer)

Cutri, R. M., et al. 2003, The IRSA 2MASS All-Sky Point Source Catalog, NASA/IPAC Infrared Science Archive

da Silva, L., et al. 2006, A&A, 458, 609

de Ridder, J., Barban, C., Carrier, F., Mazumdar, A., Eggenberger, P., Aerts, C., Deruyter, S., & Vanautgaerden, J. 2006, A&A, 448, 689

Döllinger, M. P. 2008, Ph.D., LMU Munich

Döllinger, M. P., Hatzes, A. P., Pasquini, L., Guenther, E. W., Hartmann, M., Girardi, L., & Esposito, M. 2007, A&A, 472, 649

Döllinger, M.P., Hatzes, A.P., Pasquini, L., Guenther, E.W., Hartmann, M., & Girardi, L. 2009a, A&A, 499, 935

Döllinger, M.P., Hatzes, A.P., Pasquini, L., Guenther, E.W., & Hartmann, M. 2009b, resubmitted

Döllinger, M.P., Hatzes, A.P., Pasquini, L., Guenther, E.W., & Hartmann, M. 2009c, in preparation

Döllinger, M.P., Hatzes, A.P., Pasquini, L., Guenther, E.W., & Hartmann, M. 2009d, in preparation

ESA 1997, VizieR Online Data Catalog, 1239, 0

Famaey, B., Jorissen, A., Luri, X., Mayor, M., Udry, S., Dejonghe, H., & Turon, C. 2005, A&A, 430, 165

Fitzpatrick, E. L. 1999, PASP, 111, 63

Frandsen, S., et al. 2002, A&A, 394, L5

Girardi, L., Bressan, A., Bertelli, G., & Chiosi, C. 2000, A&AS, 141, 371

Gustafsson, B., Bell, R. A., Eriksson, K., & Nordlund, A. 1975, A&A, 42, 407

Hanbury-Brown, R., Davis, J., Lake, R. J. W., & Thompson, R. J. 1974, MNRAS, 167, 475

Hatzes, A. P., & Cochran, W. D. 1994, ApJ, 422, 366

Hatzes, A.P., et al. 2006, A&A, 457, 335

Hatzes, A. P., & Zechmeister M. 2007, ApJ, 670, L37

Johnson, J. A., Marcy, G. W., Fischer, D. A., Wright, J. T., Reffert, S., Kregenow, J. M., Williams, P. K. G., & Peek, K. M. G. 2008, ApJ, 675, 784

Kervella, P., Thévenin, F., Di Folco, E., & Ségransan, D. 2004, A&A, 426, 297

McAlister, H. A., et al. 2005, ApJ, 628, 439

Mermilliod, J. C. 1991, *Catalogue of Homogeneous Means in the UBV System*, Institut d'Astronomie, Universite de Lausanne

Monet, D. G., et al. 2003, AJ, 125, 984

Morel, M., & Magnenat, P. 1978, A&AS, 34, 477

Mozurkewich, D., et al. 2003, AJ, 126, 2502

Neugebauer, G., & Leighton, R. B. 1969, NASA SP, Washington: NASA, 1969

Niedzielski, A., Goździewski, K., Wolszczan, A., Konacki, M., Nowak, G., & Zieliński, P. 2009, ApJ, 693, 276

Nordgren, T. E., et al. 1999, AJ, 118, 3032

Nordgren, T. E., Sudol, J. J., & Mozurkewich, D. 2001, AJ, 122, 2707 1

Pasquini, L., Bonifacio, P., Randich, S., Galli, D., & Gratton, R. G. 2004, A&A, 426, 651

Press, W. H., Teukolsky, S. A., Vetterling, W. T., & Flannery, B. P. 1992, Numerical recipes in C. The art of scientific computing (Cambridge: University Press, c1992, 2nd ed.)

Sato, B., Kambe, E., Takeda, Y., Izumiura, H., Masuda, S., & Ando, H. 2005, PASJ, 57, 97

Sato, B., et al. 2008, PASJ, 60, 1317

Setiawan, J., et al. 2005, A&A, 437, L31

Shao, M., & Colavita, M. M. 1992, ARA&A, 30, 457

Short, C. I., & Hauschildt, P. H. 2009, ApJ, 691, 1634

Teixeira, T. C., et al. 2009, A&A, 494, 237

ten Brummelaar, T. A., et al. 2005, ApJ, 628, 453

van Belle, G. T., et al. 1999, AJ, 117, 521

van Leeuwen, F. 2007, Hipparcos, the New Reduction of the Raw Data (Cambridge, UK Series: Astrophysics and Space Science Library; Springer)

Wall, J. V., & Jenkins, C. R. 2003, Practical Statistics for Astronomers (Princeton Series in Astrophysics)

This preprint was prepared with the AAS LaTeX macros v5.2.

Table 1. Observed and Spectroscopic Properties of the K Giants.

Target HD	V mag	K mag	Spec Type	π (mas)	$T_{\rm eff}$ ±70 K	log g ±0.2	[Fe/H] ±0.5 dex	$\theta_{\rm estimate}$ (mas)	$R_{\rm estimate}$ ($R_\odot$)	$M_{\rm estimate}$ ($M_\odot$)
32518	6.41	3.91 ± 0.04^a	K1 III	8.29 ± 0.58	4580	2.0	-0.15	0.84 ± 0.05	10.9 ± 1.0	1.1 ± 0.2
60294	5.92	3.55 ± 0.22^a	K2 III	12.24 ± 0.39	4520	2.4	+0.02	0.97 ± 0.31	8.5 ± 2.7	1.2 ± 0.1
73108	4.60	1.92 ± 0.07^b	K1 III	12.74 ± 0.26	4415	1.8	-0.25	2.17 ± 0.22	18.3 ± 1.9	1.2 ± 0.2
102328	5.29	2.55 ± 0.06^b	K3 III	15.13 ± 0.30	4250	1.9	+0.09	1.64 ± 0.14	11.6 ± 1.0	1.1 ± 0.1
103605	5.84	3.10 ± 0.30^a	K1 III	10.54 ± 0.37	4740	2.8	-0.07	1.27 ± 0.54	12.9 ± 5.5	1.1 ± 0.2
106574	5.71	2.94 ± 0.08^b	K2 III	7.00 ± 0.28	4570	2.2	-0.31	1.38 ± 0.16	21.1 ± 2.6	1.6 ± 0.2
113049	6.00	3.66 ± 0.31^a	K0 III	6.02 ± 0.37	4740	2.2	-0.18	0.92 ± 0.41	16.4 ± 7.3	2.2 ± 0.3
118904	5.51	2.69 ± 0.07^b	K2 III	7.93 ± 0.24	4500	2.2	-0.18	1.55 ± 0.16	21.1 ± 2.2	1.4 ± 0.2
136726	5.01	1.92 ± 0.05^b	K4 III	8.19 ± 0.19	4340	1.6	+0.04	2.33 ± 0.17	30.5 ± 2.4	2.0 ± 0.2
137443	5.79	2.74 ± 0.06^b	K4 III	8.86 ± 0.22	4435	2.6	-0.03	1.58 ± 0.14	19.2 ± 1.7	1.4 ± 0.2
138265	5.88	2.38 ± 0.04^b	K5 III	5.11 ± 0.31	4200	2.4	-0.07	2.02 ± 0.12	42.5 ± 3.6	1.5 ± 0.2
139357	5.97	3.41 ± 0.32^a	K4 III	8.47 ± 0.30	4700	2.9	-0.13	1.07 ± 0.49	13.6 ± 6.2	1.3 ± 0.2
150010	6.28	3.18 ± 0.38^a	K2 III	6.95 ± 0.43	4540	2.8	-0.02	1.31 ± 0.71	20.2 ± 11.1	1.4 ± 0.3
152812	6.00	2.83 ± 0.09^b	K2 III	4.97 ± 0.45	4220	1.4	-0.42	1.55 ± 0.20	33.5 ± 5.3	1.1 ± 0.1
157681	5.67	2.19 ± 0.05^b	K5 III	5.23 ± 0.27	4400	1.6	-0.23	2.20 ± 0.16	45.2 ± 4.1	1.7 ± 0.3
160290	5.36	2.67 ± 0.07^b	K1 III	9.23 ± 0.21	4750	2.7	-0.17	1.54 ± 0.16	17.9 ± 1.9	2.0 ± 0.3
167042	5.98	3.55 ± 0.24^a	K1 III	19.91 ± 0.26	4820	2.9	-0.08	0.98 ± 0.33	5.3 ± 1.8	1.2 ± 0.1
170693	4.83	1.95 ± 0.05^b	K1.5 III	10.36 ± 0.20	4200	1.0	-0.46	2.21 ± 0.16	22.9 ± 1.7	1.0 ± 0.1
175823	6.22	3.57 ± 0.32^a	K5 III	5.63 ± 0.28	4500	2.1	-0.12	1.01 ± 0.46	19.2 ± 8.7	1.7 ± 0.2
176408	5.66	3.00 ± 0.27^a	K1 III	11.81 ± 0.27	4500	2.3	-0.06	1.31 ± 0.50	12.0 ± 4.6	1.1 ± 0.2
186815	6.28	4.32 ± 0.25^a	K2 III	12.86 ± 0.39	4900	2.5	-0.32	0.63 ± 0.23	5.3 ± 1.9	1.2 ± 0.1
192781	5.79	2.33 ± 0.07^b	K5 III	5.62 ± 0.23	4210	2.3	-0.08	2.05 ± 0.21	39.3 ± 4.3	1.4 ± 0.2
195820	6.18	3.90 ± 0.22^a	K0 III	8.68 ± 0.29	4710	2.4	-0.16	0.81 ± 0.25	10.1 ± 3.2	1.0 ± 0.2
200205	5.51	2.25 ± 0.06^b	K4 III	5.30 ± 0.24	4210	1.6	-0.28	2.06 ± 0.18	41.7 ± 4.1	1.3 ± 0.2
214868	4.48	1.41 ± 0.07^b	K2 III	9.80 ± 0.26	4440	2.1	-0.18	2.93 ± 0.30	32.1 ± 3.4	1.8 ± 0.2

Note. — [a] *2MASS All-Sky Catalog of Point Sources* (Cutri et al. 2003); [b] *Two-Micron Sky Survey* (Neugebauer & Leighton 1969); V magnitudes are from Mermilliod (1991) and spectral types are from the *SIMBAD Astronomical Database*; parallaxes (π) are from van Leeuwen (2007); $T_{\rm eff}$, log g, [Fe/H] from Döllinger (2008); $\theta_{\rm estimate}$ and $R_{\rm estimate}$ were determined photometrically, and $M_{\rm estimate}$ is from the PARAM Stellar Model (da Silva et al. 2006).

Table 2. Observing Log and Calibrator Stars' Basic Parameters.

Observing Log					Calibrator Information		
Target HD	Calibrator HD	Baseline† (max. length)	Date (UT)	# Obs	$T_{\rm eff}$‡ (K)	log g‡ (cm s^{-2})	$\theta_{\rm LD}$* (mas)
32518	31675	S1-E1 (331 m)	2007/11/14	9	6310	4.39	0.401±0.015
60294	63332	S1-E1 (331 m)	2009/04/23	5	6310	4.19	0.431±0.014
	69548			5	6761	4.31	0.402±0.018
73108	69548	E2-W2 (156 m)	2008/05/09	5	6761	4.31	0.402±0.018
102328	98673	S1-E1 (331 m)	2009/04/24	3	8128	4.21	0.220±0.010
	108954			2	6026	4.34	0.452±0.021
103605	108954	S1-E1 (331 m)	2009/04/22	4	6026	4.34	0.452±0.021
	98673		2009/04/24	3	8128	4.21	0.220±0.010
	108954			3	6026	4.34	0.452±0.021
106574	107193	E2-W2 (156 m)	2008/06/29	6	8710	3.93	0.315±0.030
113049	107193	S1-E1 (331 m)	2009/04/23	8	8710	3.93	0.315±0.030
	124063			5	7740	4.29	0.232±0.010
118904	124063	E2-W2 (156 m)	2008/06/29	6	7740	4.29	0.232±0.010
136726	145454	E2-W2 (156 m)	2008/05/09	6	9772	4.13	0.268±0.015
137443	145454	E2-W2 (156 m)	2008/05/09	6	9772	4.13	0.268±0.015
138265	145454	E2-W2 (156 m)	2008/05/09	4	9772	4.13	0.268±0.015
			2008/05/11	3			
139357	132254	S1-E1 (331 m)	2007/09/14	4	6310	4.27	0.521±0.015
			2007/09/15	3			
150010	145454	E2-W2 (156 m)	2008/06/29	6	9772	4.13	0.268±0.015
	149681	S1-E1 (331 m)	2008/07/17	4	7586	4.23	0.368±0.012
152812	149303	S1-E1 (331 m)	2009/04/20	4	8511	4.10	0.288±0.011
	151044			5	6166	4.38	0.380±0.008
157681	158460	S1-E1 (331 m)	2007/09/14	5	9000	4.19	0.268±0.016
160290	158414	S1-E1 (331 m)	2009/04/24	6	8000	4.24	0.295±0.012
	161693			4	9000	4.19	0.258±0.015
167042	161693	S1-E1 (331 m)	2007/09/15	8	9000	4.19	0.258±0.015
170693	172569	W1-S2 (249 m)	2007/09/03	4	7413	3.98	0.309±0.013
175823	172728	S1-E1 (331 m)	2009/04/23	4	9790	4.14	0.236±0.020

Table 2—Continued

Observing Log					Calibrator Information		
Target HD	Calibrator HD	Baseline† (max. length)	Date (UT)	# Obs	$T_{\rm eff}$‡ (K)	log g‡ (cm s^{-2})	$\theta_{\rm LD}$* (mas)
	178207			6	9790	4.14	0.271±0.015
176408	172728	S1-E1 (331 m)	2009/04/23	4	9790	4.14	0.236±0.020
	178207			6	9790	4.14	0.271±0.015
186815	186760	S1-E1 (331 m)	2009/04/24	7	6026	3.90	0.432±0.019
	188793			9	8800	4.21	0.226±0.016
192781	186760	S1-E1 (331 m)	2009/04/24	7	6026	3.90	0.432±0.019
	188793			9	8800	4.21	0.226±0.016
195820	184960	S1-E1 (331 m)	2007/11/14	4	6457	4.33	0.492±0.019
200205	197950	W1-S2 (249 m)	2007/09/03	8	7762	4.30	0.349±0.014
214868	211211	E2-W2 (156 m)	2008/06/29	4	9333	4.17	0.249±0.015
		S1-E1 (331 m)	2008/07/01	3			

Note. — †The three arms of the Array are denoted by their cardinal directions: "S" is south, "E" is east, and "W" is west. Each arm bears two telescopes, numbered "1" for the telescope farthest from the beam combining laboratory and "2" for the telescope closer to the lab.

‡All $T_{\rm eff}$ and log g values are from Allende Prieto & Lambert (1999) except for HD 124063, HD 158414, HD 158460, HD 161693, HD 172728, HD 178207, and HD 188793, which are from Cox (2000) and were based on their spectral types as listed in the *SIMBAD Astronomical Database*.

*In calculating $\theta_{\rm LD}$ as described in §3, the UBV values were from Mermilliod (1991) except for HD 149303 (ESA 1997), and HD 151044 and HD 184960 (Morel & Magnenat 1978); all RI values were from Monet et al. (2003) except for HD 151044 and HD 184960 (Morel & Magnenat 1978); and all JHK values were from Cutri et al. (2003).

Table 3. K Giants' Calibrated Visibilities.

Target HD	Calib HD	MJD	B (m)	Θ (deg)	V_c	σV_c
32518	31675	54418.238	230.84	200.1	0.755	0.067
		54418.244	233.56	201.8	0.794	0.071
		54418.250	236.48	203.6	0.834	0.070
		54418.256	239.18	205.3	0.843	0.074
		54418.261	241.66	206.9	0.751	0.061
		54418.267	244.20	208.6	0.743	0.053
		54418.274	246.86	210.3	0.776	0.059
		54418.280	249.36	212.0	0.741	0.065
		54418.286	251.81	213.8	0.732	0.053
60294	63332	54944.176	319.48	94.9	0.444	0.045
		54944.184	319.22	96.9	0.451	0.054
		54944.192	318.88	98.9	0.474	0.036
		54944.201	318.44	100.8	0.481	0.035
		54944.208	317.93	102.7	0.449	0.058
	69548	54944.160	319.72	91.0	0.526	0.057
		54944.168	319.64	92.9	0.448	0.057
		54944.192	318.88	98.9	0.485	0.040
		54944.201	318.44	100.8	0.505	0.052
		54944.208	317.93	102.7	0.455	0.053
73108	69548	54595.216	155.95	254.7	0.411	0.051
		54595.226	155.88	258.0	0.446	0.034
		54595.235	155.83	261.1	0.436	0.043
		54595.244	155.80	264.1	0.460	0.057
		54595.257	155.77	268.4	0.430	0.092
102328	98673	54945.239	314.63	248.9	0.086	0.011
		54945.252	316.18	252.0	0.088	0.009
		54945.290	319.04	261.0	0.073	0.011
	108954	54945.239	314.63	248.9	0.100	0.012
		54945.264	317.31	254.8	0.095	0.012
103605	108954	54943.375	317.53	99.1	0.437	0.027
		54943.382	317.18	100.6	0.442	0.032

Table 3—Continued

Target HD	Calib HD	MJD	B (m)	Θ (deg)	V_c	σV_c
		54943.388	316.77	102.2	0.457	0.038
		54943.394	316.37	103.5	0.409	0.029
	98673	54945.242	312.54	248.0	0.445	0.048
		54945.255	314.17	251.0	0.410	0.040
		54945.280	316.51	256.9	0.446	0.062
	108954	54945.267	315.40	253.8	0.465	0.069
		54945.280	316.51	256.9	0.489	0.054
		54945.293	317.37	260.2	0.449	0.044
106574	107193	54646.187	155.91	241.7	0.699	0.099
		54646.196	155.99	244.8	0.698	0.131
		54646.205	156.06	247.8	0.741	0.098
		54646.214	156.11	250.8	0.680	0.086
		54646.223	156.14	253.9	0.732	0.085
		54646.234	156.18	257.5	0.701	0.081
113049	107193	54944.362	272.32	265.1	0.655	0.059
		54944.370	272.47	267.4	0.630	0.051
		54944.378	272.53	269.5	0.692	0.070
		54944.386	272.50	91.9	0.670	0.052
		54944.394	272.37	94.4	0.587	0.049
		54944.403	272.12	96.8	0.605	0.049
		54944.411	271.80	99.0	0.633	0.076
		54944.419	271.38	101.3	0.696	0.071
	124063	54944.362	272.32	265.1	0.611	0.059
		54944.370	272.47	267.4	0.542	0.035
		54944.378	272.53	269.5	0.602	0.048
		54944.411	271.80	99.0	0.581	0.070
		54944.419	271.38	101.3	0.656	0.058
118904	124063	54646.251	155.81	244.4	0.574	0.074
		54646.260	155.89	247.3	0.567	0.069
		54646.268	155.95	250.1	0.589	0.060
		54646.278	156.01	253.3	0.512	0.064

Table 3—Continued

Target HD	Calib HD	MJD	B (m)	Θ (deg)	V_c	σV_c
		54646.288	156.05	256.6	0.583	0.070
		54646.297	156.08	259.6	0.562	0.088
136726	145454	54595.294	147.57	189.4	0.442	0.055
		54595.307	148.79	193.7	0.425	0.045
		54595.315	149.53	196.5	0.468	0.054
		54595.325	150.30	199.6	0.421	0.056
		54595.336	151.17	203.4	0.436	0.062
		54595.346	151.80	206.5	0.409	0.053
137443	145454	54595.385	155.65	219.1	0.673	0.082
		54595.394	155.90	222.1	0.631	0.083
		54595.404	156.07	225.1	0.616	0.063
		54595.415	156.20	228.5	0.605	0.068
		54595.430	156.26	233.6	0.656	0.077
		54595.440	156.24	236.6	0.664	0.048
138265	145454	54595.455	155.83	240.4	0.542	0.081
		54595.466	155.64	243.8	0.578	0.130
		54595.476	155.45	247.1	0.494	0.085
		54595.488	155.23	251.0	0.467	0.070
		54597.467	155.50	246.2	0.559	0.079
		54597.477	155.33	249.3	0.500	0.061
		54597.486	155.16	252.4	0.478	0.061
139357	132254	54357.149	320.57	102.8	0.450	0.070
		54357.155	320.14	104.2	0.460	0.045
		54357.161	319.66	105.6	0.487	0.063
		54357.167	319.12	107.1	0.491	0.066
		54358.151	320.24	103.9	0.460	0.030
		54358.157	319.77	105.3	0.415	0.034
		54358.162	319.27	106.7	0.429	0.049
150010	145454	54646.318	154.39	226.3	0.785	0.122
		54646.327	154.64	229.1	0.836	0.103
		54646.335	154.85	231.9	0.823	0.085

Table 3—Continued

Target HD	Calib HD	MJD	B (m)	Θ (deg)	V_c	σV_c
		54646.345	155.07	235.1	0.835	0.113
		54646.354	155.24	238.2	0.862	0.125
		54646.363	155.39	241.1	0.822	0.083
	149681	54664.392	273.81	117.3	0.583	0.086
		54664.403	272.04	120.2	0.589	0.096
		54664.413	270.21	123.0	0.640	0.080
		54664.423	268.16	125.8	0.724	0.125
152812	149303	54941.490	327.27	256.0	0.152	0.014
		54941.499	327.63	257.9	0.164	0.015
		54941.507	327.94	259.9	0.154	0.010
		54941.516	328.18	261.9	0.148	0.015
	151044	54941.481	326.75	253.8	0.158	0.017
		54941.490	327.27	256.0	0.144	0.014
		54941.499	327.63	257.9	0.168	0.015
		54941.507	327.94	259.9	0.157	0.011
		54941.516	328.18	261.9	0.154	0.016
157681	158460	54357.211	321.92	99.9	0.056	0.004
		54357.221	321.36	102.3	0.056	0.005
		54357.231	320.64	104.8	0.057	0.005
		54357.241	319.83	107.1	0.060	0.004
		54357.251	318.83	109.4	0.060	0.010
160290	158414	54945.330	279.04	219.2	0.267	0.020
		54945.339	283.87	220.7	0.280	0.030
		54945.348	288.23	222.2	0.247	0.030
		54945.356	292.52	223.8	0.250	0.037
		54945.366	296.96	225.7	0.217	0.042
		54945.375	300.60	227.4	0.172	0.022
	161693	54945.348	288.23	222.2	0.225	0.026
		54945.356	292.52	223.8	0.228	0.027
		54945.366	296.96	225.7	0.183	0.021
		54945.375	300.60	227.4	0.167	0.017

Table 3—Continued

Target HD	Calib HD	MJD	B (m)	Θ (deg)	V_c	σV_c
167042	161693	54358.232	321.20	97.5	0.584	0.037
		54358.238	320.96	99.0	0.551	0.036
		54358.243	320.68	100.3	0.507	0.036
		54358.249	320.34	101.7	0.524	0.030
		54358.255	319.96	103.1	0.571	0.036
		54358.261	319.53	104.5	0.612	0.037
		54358.267	319.05	105.9	0.591	0.041
		54358.273	318.48	107.4	0.627	0.050
170693	172569	54346.303	187.40	183.8	0.373	0.042
		54346.311	183.87	186.6	0.343	0.049
		54346.321	179.32	190.2	0.358	0.037
		54346.332	174.70	193.9	0.457	0.042
175823	172728	54944.471	297.24	232.9	0.499	0.044
		54944.482	300.30	235.4	0.480	0.064
		54944.493	303.23	238.1	0.553	0.065
		54944.505	305.73	240.8	0.533	0.056
	178207	54944.442	287.69	226.5	0.633	0.071
		54944.454	291.73	229.0	0.667	0.053
		54944.471	297.24	232.9	0.590	0.052
		54944.482	300.30	235.4	0.576	0.082
		54944.493	303.23	238.1	0.569	0.060
		54944.505	305.73	240.8	0.580	0.045
176408	172728	54944.473	296.67	232.9	0.409	0.043
		54944.484	299.83	235.5	0.409	0.047
		54944.496	302.66	238.1	0.436	0.059
		54944.507	305.17	240.8	0.416	0.046
	178207	54944.445	287.23	226.5	0.585	0.060
		54944.456	291.14	228.9	0.587	0.055
		54944.473	296.67	232.9	0.501	0.053
		54944.484	299.83	235.5	0.462	0.058
		54944.496	302.66	238.1	0.452	0.057

Table 3—Continued

Target HD	Calib HD	MJD	B (m)	Θ (deg)	V_c	σV_c
		54944.507	305.17	240.8	0.465	0.039
186815	186760	54945.396	248.69	209.6	0.792	0.082
		54945.408	256.16	212.2	0.891	0.083
		54945.419	262.58	214.5	0.732	0.056
		54945.429	268.32	216.8	0.777	0.069
		54945.440	273.75	219.1	0.764	0.072
		54945.484	292.08	228.8	0.815	0.053
		54945.495	295.81	231.3	0.740	0.058
	188793	54945.396	248.69	209.6	0.749	0.098
		54945.408	256.16	212.2	0.929	0.111
		54945.419	262.58	214.5	0.760	0.082
		54945.429	268.32	216.8	0.699	0.075
		54945.440	273.75	219.1	0.742	0.069
		54945.461	283.52	223.8	0.783	0.058
		54945.473	287.96	226.3	0.778	0.040
		54945.484	292.08	228.8	0.761	0.044
		54945.495	295.81	231.3	0.726	0.057
192781	186760	54945.400	231.04	202.6	0.225	0.027
		54945.411	238.31	205.2	0.202	0.017
		54945.422	245.12	207.9	0.174	0.012
		54945.432	251.29	210.4	0.172	0.014
		54945.443	257.29	212.9	0.140	0.012
		54945.487	277.78	223.2	0.078	0.005
		54945.498	282.14	225.9	0.062	0.004
	188793	54945.400	231.04	202.6	0.220	0.032
		54945.411	238.31	205.2	0.214	0.024
		54945.422	245.12	207.9	0.173	0.018
		54945.432	251.29	210.4	0.154	0.016
		54945.443	257.29	212.9	0.143	0.012
		54945.464	268.07	218.0	0.109	0.010
		54945.476	273.15	220.6	0.091	0.006

Table 3—Continued

Target HD	Calib HD	MJD	B (m)	Θ (deg)	V_c	σV_c
		54945.487	277.78	223.2	0.074	0.004
		54945.498	282.14	225.9	0.062	0.004
195820	184960	54418.169	323.56	98.4	0.626	0.070
		54418.184	322.84	102.0	0.703	0.076
		54418.194	322.25	104.2	0.546	0.051
		54418.203	321.50	106.5	0.610	0.059
200205	197950	54346.350	214.19	161.4	0.327	0.032
		54346.358	211.24	163.5	0.309	0.039
		54346.365	208.36	165.4	0.267	0.030
		54346.372	205.28	167.4	0.302	0.039
		54346.378	202.26	169.3	0.338	0.033
		54346.385	199.22	171.2	0.242	0.021
		54346.392	195.69	173.3	0.267	0.035
		54346.406	188.87	177.4	0.318	0.031
214868	211211	54646.402	138.11	183.1	0.361	0.072
		54646.413	141.40	185.6	0.352	0.042
		54646.423	144.26	188.0	0.326	0.054
		54646.433	146.89	190.5	0.304	0.058
		54648.457	322.39	239.2	0.073	0.012
		54648.469	324.32	241.8	0.064	0.005
		54648.479	325.51	243.8	0.079	0.007

Note. — The projected baseline position angle (Θ) is calculated to be east of north.

Table 4. Interferometric Diameter and Effective Temperature Measurements of the K Giants.

Target HD	$\theta_{\rm UD,interferometric}$ (mas)	$\theta_{\rm LD,interferometric}$ (mas)	$\sigma_{\rm LD}$ (%)	$R_{\rm linear}$ ($R_\odot$)	$A_{\rm V}$	BC	$L_\star$ ($L_\odot$)	$F_{\rm BOL}$ (10^{-8} erg s^{-1} cm^{-2})	$T_{\rm eff}$ (K)	$\sigma_{\rm Teff}$ %
32518	0.828 ± 0.022	0.851 ± 0.022	3	11.04 ± 0.77	0.06	0.43 ± 0.08	49.2 ± 3.6	10.8 ± 0.9	4600 ± 112	2
60294	1.014 ± 0.010	1.044 ± 0.010	1	9.17 ± 0.29	0.05	0.35 ± 0.06	32.5 ± 1.9	15.6 ± 1.0	4552 ± 74	2
73108	2.161 ± 0.019	2.225 ± 0.020	1	18.79 ± 0.38	0.00	0.51 ± 0.09	112.4 ± 10.0	58.3 ± 5.2	4336 ± 99	2
102328	1.546 ± 0.006	1.606 ± 0.006	0.4	11.42 ± 0.23	0.00	0.51 ± 0.09	42.4 ± 3.8	31.0 ± 2.8	4358 ± 97	2
103605	1.066 ± 0.009	1.098 ± 0.010	1	11.20 ± 0.41	0.00	0.52 ± 0.09	52.9 ± 4.8	18.8 ± 1.7	4651 ± 109	2
106574	1.458 ± 0.027	1.498 ± 0.028	2	23.02 ± 0.92	0.00	0.54 ± 0.10	136.6 ± 12.7	21.4 ± 2.0	4113 ± 105	3
113049†	0.945 ± 0.021	0.971 ± 0.022	2	17.35 ± 1.07	0.00	0.35 ± 0.06	119.7 ± 7.2	13.9 ± 0.9	4583 ± 93	2
118904	1.842 ± 0.031	1.871 ± 0.032	2	25.38 ± 0.88	0.00	0.60 ± 0.11	136.0 ± 14.1	27.3 ± 2.9	3913 ± 108	3
136726	2.264 ± 0.020	2.336 ± 0.020	1	30.68 ± 0.76	0.04	0.70 ± 0.13	229.2 ± 28.2	49.2 ± 6.1	4055 ± 126	3
137443	1.638 ± 0.030	1.690 ± 0.031	2	20.51 ± 0.62	0.06	0.68 ± 0.12	96.1 ± 11.5	24.1 ± 2.9	3990 ± 125	3
138265	1.998 ± 0.037	2.062 ± 0.038	2	43.40 ± 2.75	0.06	0.95 ± 0.17	337.8 ± 57.5	28.2 ± 4.9	3758 ± 166	4
139357	1.040 ± 0.012	1.073 ± 0.013	1	13.63 ± 0.51	0.13	0.40 ± 0.07	73.6 ± 5.1	16.9 ± 1.2	4580 ± 86	2
150010	0.995 ± 0.028	1.024 ± 0.029	3	15.84 ± 1.08	0.04	0.70 ± 0.13	98.9 ± 12.2	15.3 ± 1.9	4572 ± 158	3
152812	1.393 ± 0.003	1.440 ± 0.004	0.3	31.16 ± 2.82	0.10	0.72 ± 0.13	270.5 ± 34.4	21.4 ± 2.9	4193 ± 142	3
157681	1.600 ± 0.009	1.664 ± 0.010	1	34.22 ± 1.78	0.04	0.94 ± 0.17	381.7 ± 64.4	33.4 ± 5.7	4361 ± 187	4
160290	1.467 ± 0.010	1.515 ± 0.010	1	17.65 ± 0.42	0.10	0.50 ± 0.09	114.4 ± 9.5	31.2 ± 2.7	4493 ± 98	2
167042	0.898 ± 0.017	0.922 ± 0.018	2	4.98 ± 0.07	0.01	0.39 ± 0.07	11.7 ± 0.8	14.8 ± 1.0	4785 ± 93	2
170693	1.981 ± 0.041	2.041 ± 0.043	2	21.19 ± 0.60	0.02	0.59 ± 0.11	149.7 ± 15.3	51.4 ± 5.3	4386 ± 122	3
175823	0.958 ± 0.022	0.988 ± 0.023	2	18.88 ± 1.04	0.05	0.49 ± 0.09	132.7 ± 11.3	13.4 ± 1.2	4509 ± 113	3
176408	1.092 ± 0.022	1.125 ± 0.023	2	10.24 ± 0.23	0.02	0.49 ± 0.09	49.2 ± 4.2	21.9 ± 1.9	4775 ± 113	2
186815	0.713 ± 0.020	0.731 ± 0.020	3	6.11 ± 0.25	0.02	0.21 ± 0.04	18.2 ± 0.7	9.6 ± 0.4	4823 ± 81	2
192781	1.787 ± 0.002	1.859 ± 0.003	0.2	35.57 ± 1.46	0.40	0.62 ± 0.11	405.2 ± 43.8	40.9 ± 4.5	4342 ± 119	3
195820	0.840 ± 0.040	0.863 ± 0.041	5	10.69 ± 0.62	0.07	0.33 ± 0.06	50.6 ± 2.8	12.2 ± 0.7	4707 ± 131	3
200205	1.963 ± 0.043	2.032 ± 0.045	2	41.23 ± 2.08	0.69	0.59 ± 0.11	569.9 ± 58.6	51.2 ± 5.4	4392 ± 125	3
214868	2.721 ± 0.020	2.731 ± 0.024	1	29.98 ± 0.84	0.15	0.69 ± 0.12	286.9 ± 34.9	88.1 ± 10.8	4339 ± 134	3

Note. — †The angular diameter and subsequent calculations are based on data calibrated using HD 107193 only. See §5 for more details.

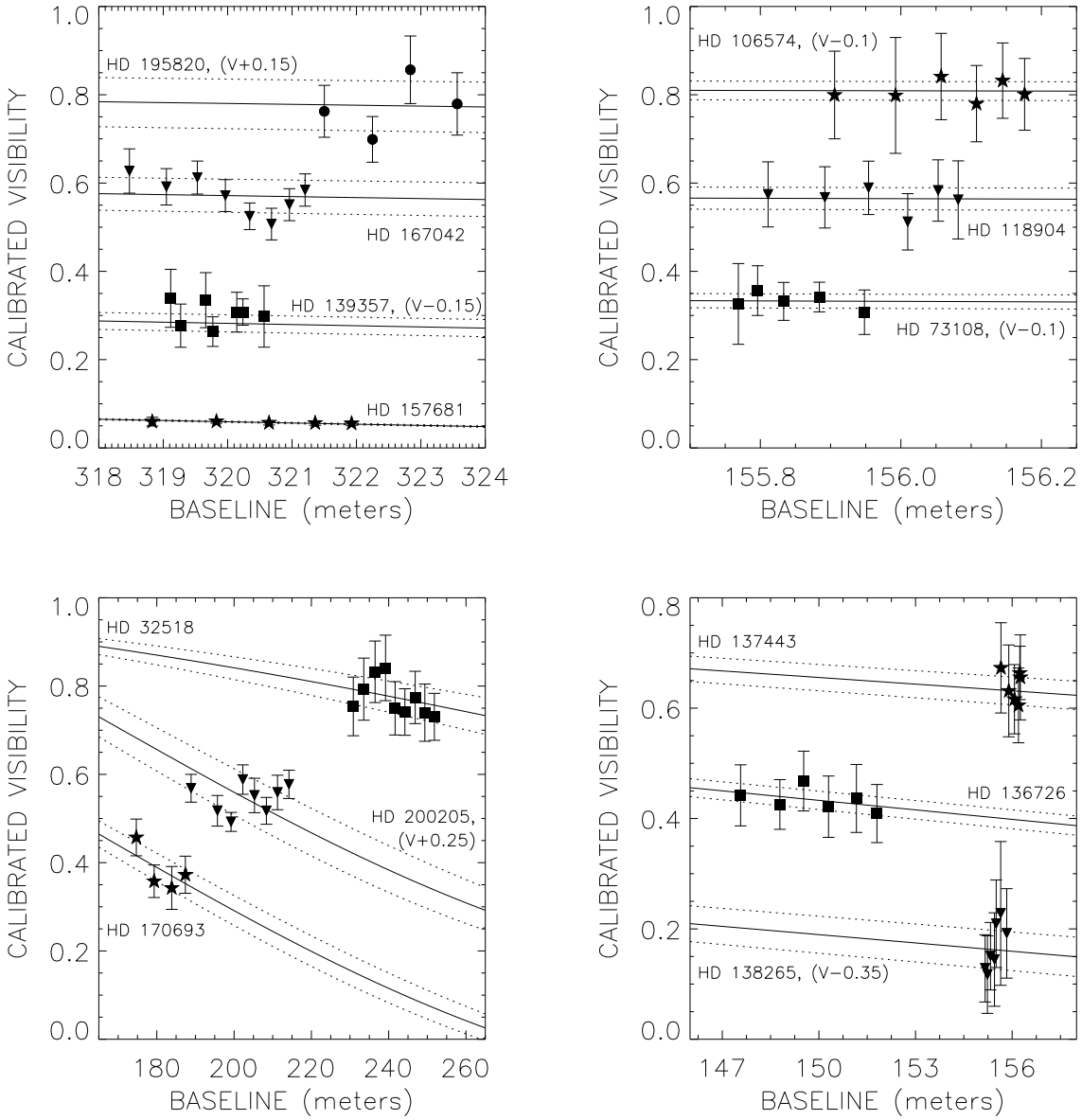

Fig. 1.— LD disk diameter fits for all the stars observed with one calibrator except HD 214868. The solid line represents the theoretical visibility curve for a star with the best fit $\theta_{\rm LD}$, the dashed lines are the 1σ error limits of the diameter fit, the solid symbols are the calibrated visibilities, and the vertical lines are the measured errors. Some of the stars' visibilities were shifted as indicated by "(V ± #)" so they would not overlap other data points.

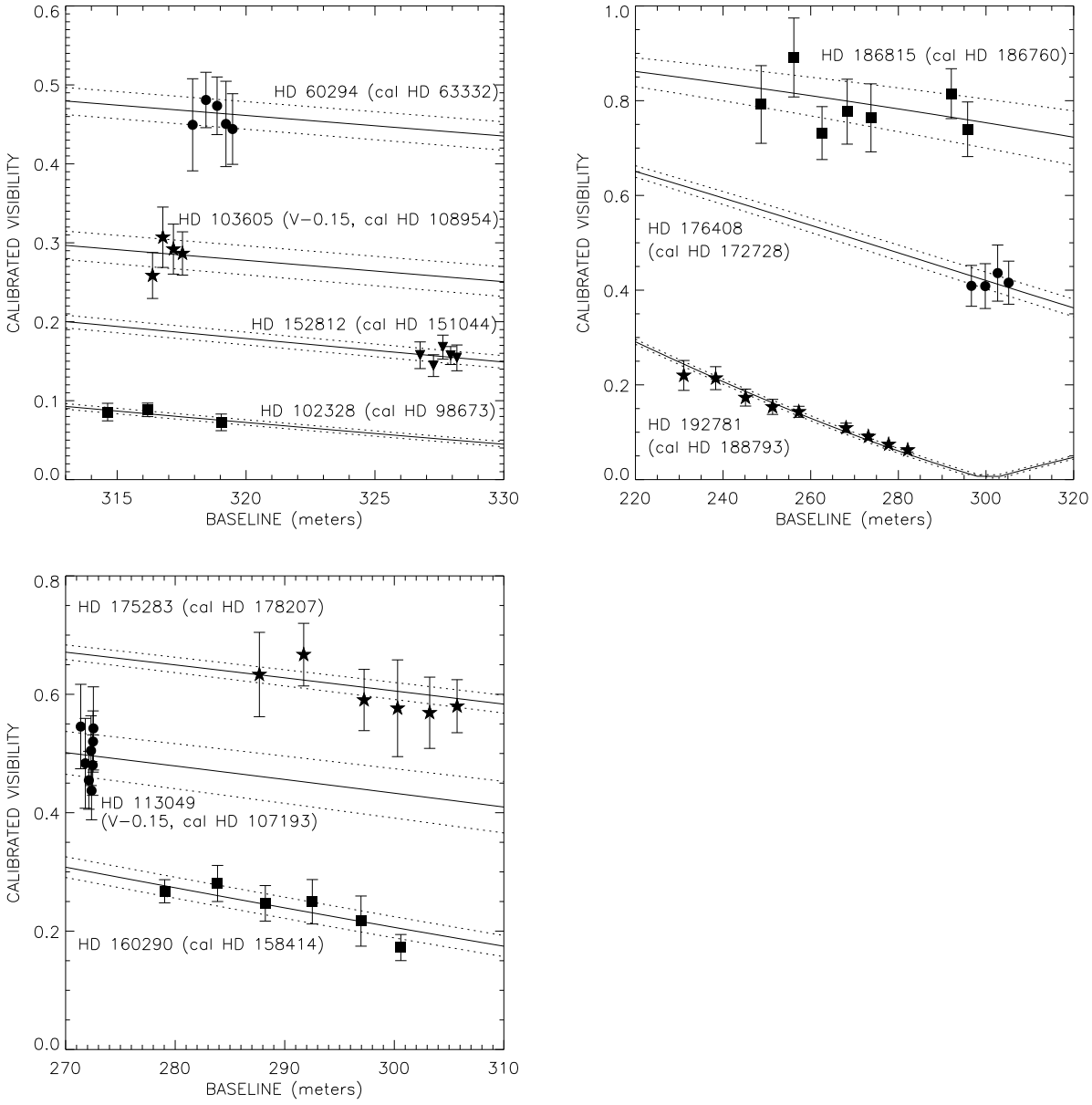

Fig. 2.— LD disk diameter fits for all the stars observed with two calibrators except HD 150010. The symbols are the same as listed in Figure 1. For the sake of clarity, the data points for one calibrator only are shown.

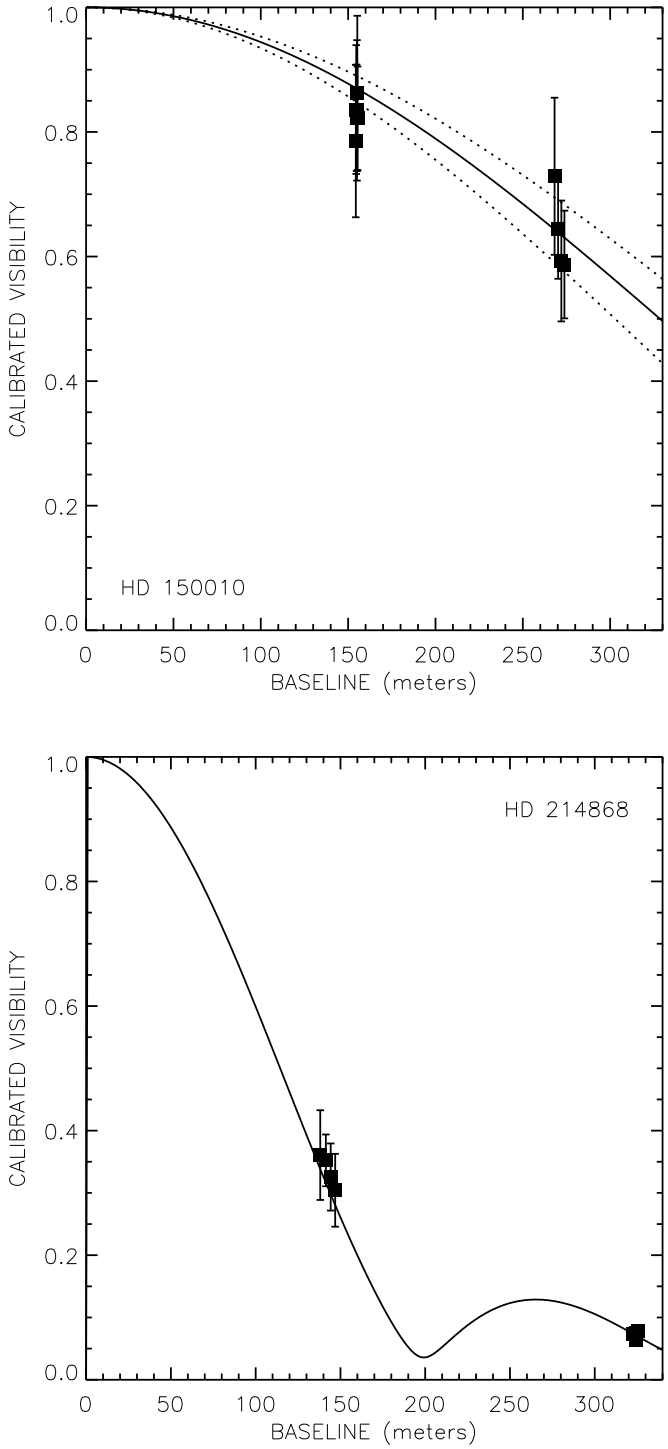

Fig. 3.— LD disk diameter fits for HD 150010 (top panel) and HD 214868 (bottom panel). The symbols are the same as listed in Figure 1.

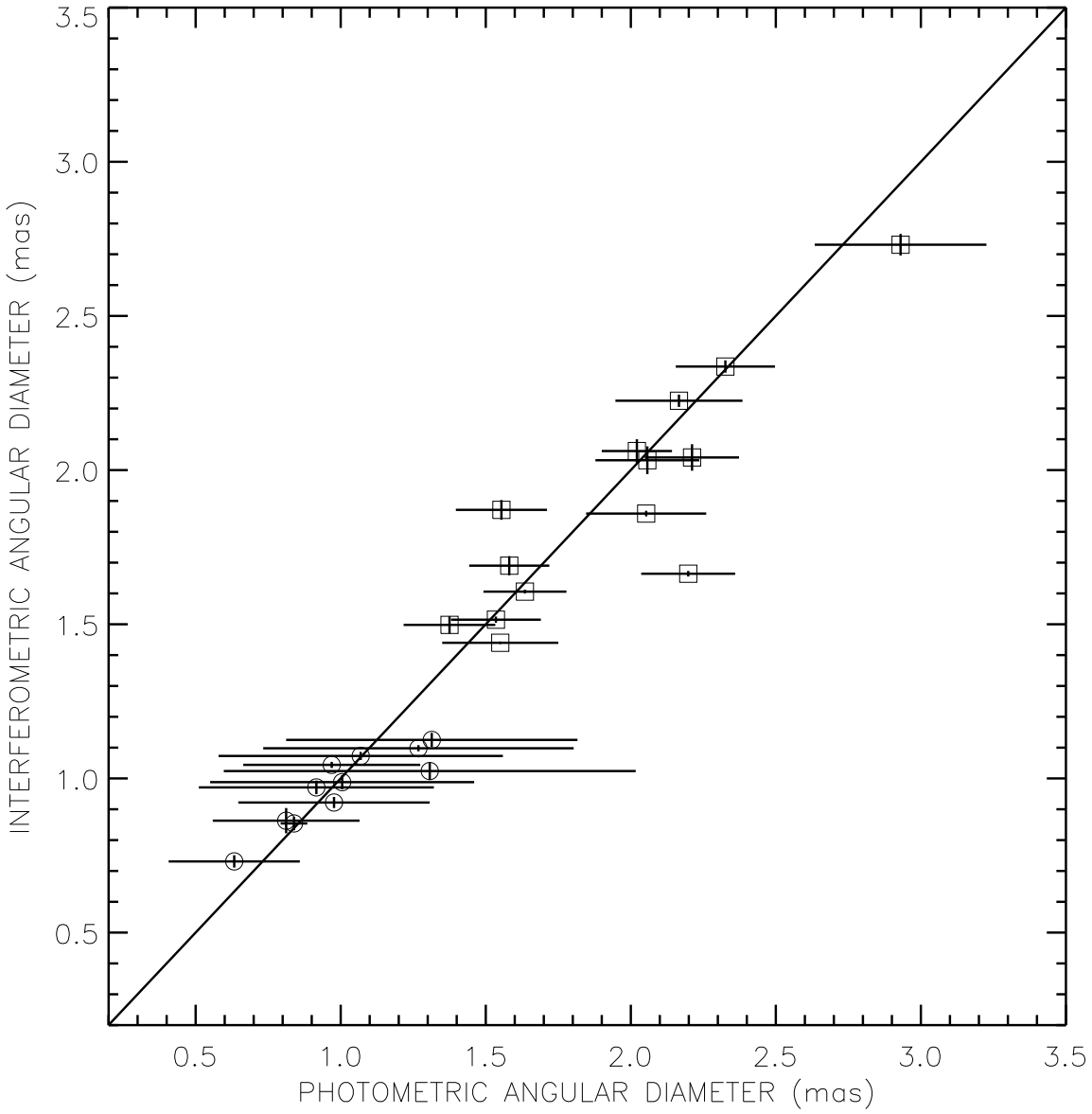

Fig. 4.— A comparison of photometrically-estimated and interferometrically-measured diameters. The squares and circles represent diameters estimated using K magnitudes from TMSS and 2MASS, respectively, and the diagonal solid line indicates a 1:1 ratio for the diameters. Note the significantly larger error bars associated with the photometric diameters, particularly those using 2MASS data. The outliers above and below the line are HD 118904 and HD 157681, respectively, and the discrepancies may be due to the calibrator used (see §5 for more details).

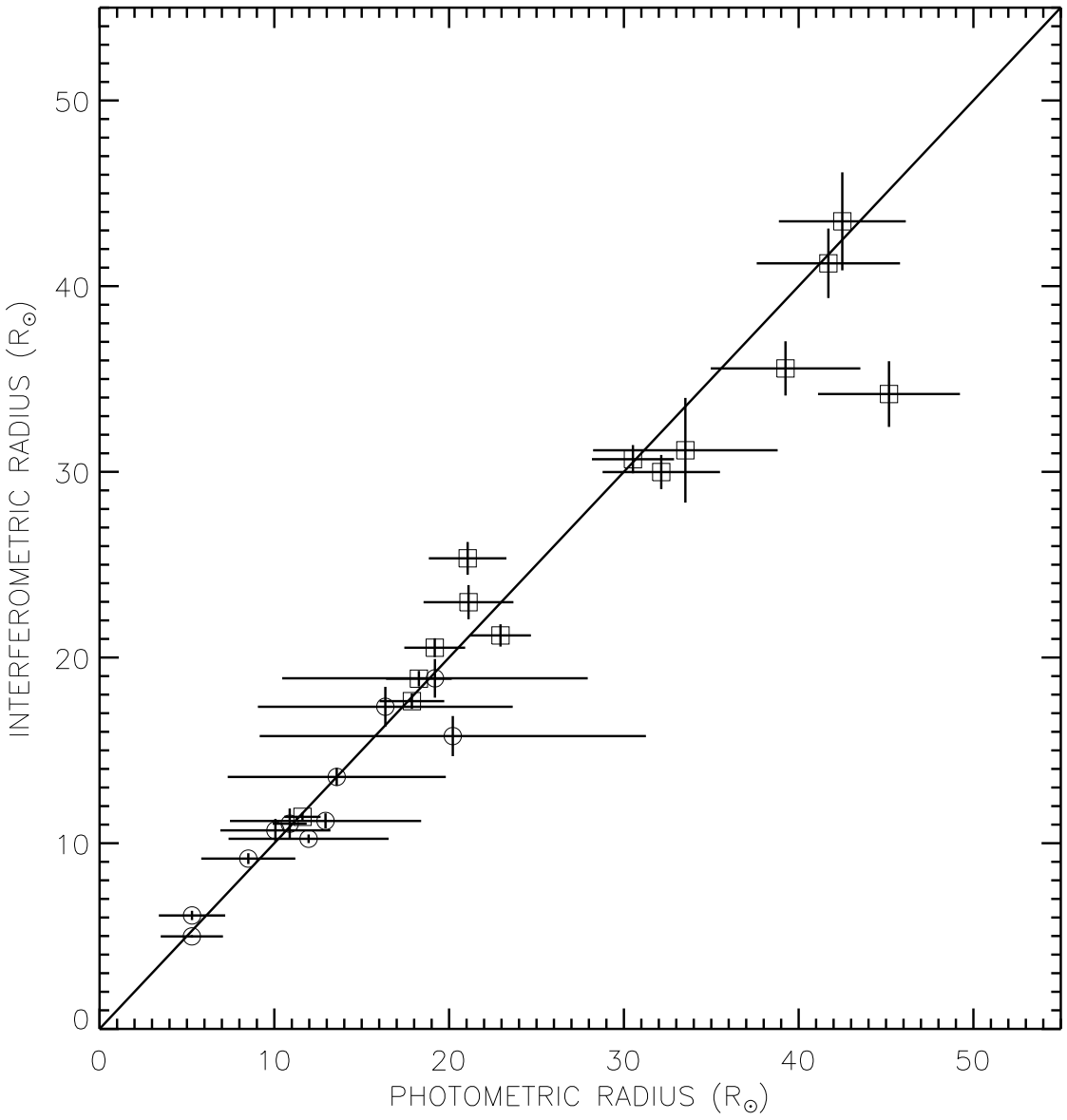

Fig. 5.— A comparison of photometrically- and interferometrically-determined linear radii. The symbols and outliers are the same as listed in Figure 4.

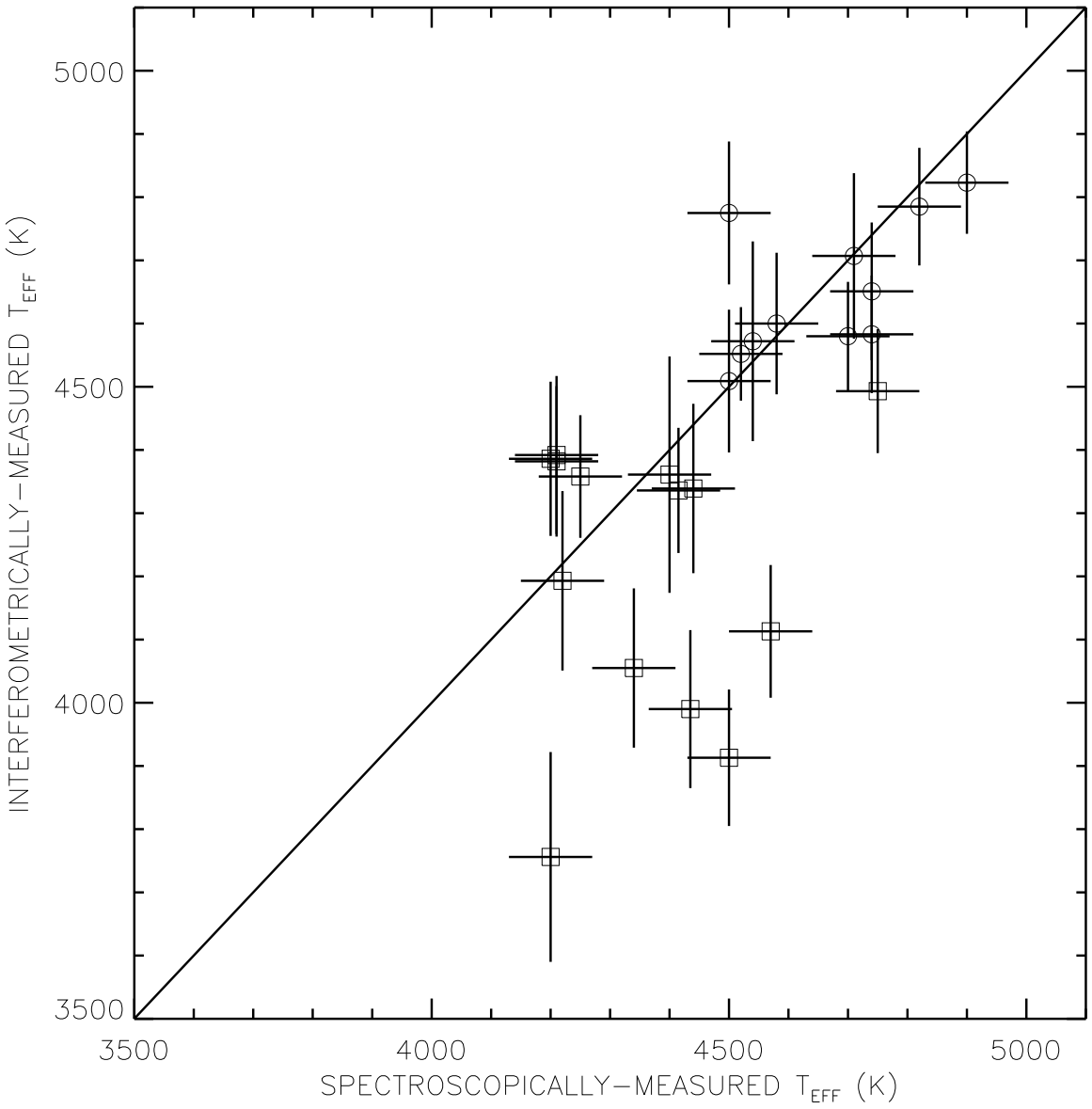

Fig. 6.— A comparison of spectroscopically- and interferometrically-measured effective temperatures. The symbols are the same as listed in Figure 4.